



Cite this: *Chem. Sci.*, 2024, **15**, 3174

All publication charges for this article have been paid for by the Royal Society of Chemistry

## Reticular chemistry guided precise construction of zirconium-pentacarboxylate frameworks with 5-connected $\text{Zr}_6$ clusters†

Tianyou Peng,<sup>‡ab</sup> Chao-Qin Han,<sup>‡a</sup> Hai-Lun Xia,<sup>a</sup> Kang Zhou,<sup>a</sup> Jian Zhang,<sup>a</sup> Jincheng Si,<sup>ca</sup> Lei Wang,<sup>a</sup> Jiafeng Miao,<sup>a</sup> Fu-An Guo,<sup>a</sup> Hao Wang,<sup>ID a</sup> Lu-Lu Qu,<sup>ID c</sup> Guozhong Xu,<sup>\*b</sup> Jing Li<sup>ID \*da</sup> and Xiao-Yuan Liu<sup>ID \*a</sup>

Zirconium-based metal–organic frameworks (Zr-MOFs) have been extensively studied due to their very rich structural chemistry. The combination of nearly unlimited carboxylic acid-based linkers and  $\text{Zr}_6$  clusters with multiple connectivities has led to diverse structures and specific properties of resultant Zr-MOFs. Herein, we demonstrate the successful use of reticular chemistry to construct two novel Zr-MOFs, HIAM-4040 and HIAM-4040-OH, with *zfu* topology. Based on a thorough structural analysis of (4,4)-connected *lvt*-type Zr-tetracarboxylate frameworks and a judicious linker design, we have obtained the first example of a Zr-pentacarboxylate framework featuring unprecedented 5-connected organic linkers and 5-connected  $\text{Zr}_6$  clusters. Compared with HIAM-4040, a larger Stokes shift is achieved in HIAM-4040-OH via hydroxyl group induced excited-state intramolecular proton transfer (ESIPT). HIAM-4040-OH exhibits high chemical and thermal stability and is used for  $\text{HClO}$  detection in aqueous solution with excellent sensitivity and selectivity.

Received 12th October 2023  
Accepted 19th January 2024

DOI: 10.1039/d3sc05410a  
[rsc.li/chemical-science](http://rsc.li/chemical-science)

## Introduction

As one of the most extensively studied subclasses, zirconium-based metal–organic frameworks (Zr-MOFs)<sup>1–6</sup> possess rich structural diversity and functionalizable sites, outstanding chemical and thermal stability, and intriguing properties. They are considered to be one of the most promising MOF branches for practical applications. The tunable linker length, number of carboxylate groups, geometry and functionality of organic linkers, and variable connection numbers of  $\text{Zr}_6$  clusters not only provide the structural abundance of Zr-MOFs, but also generate specific properties. Up to now, Zr-MOFs made of

ditopic,<sup>7–10</sup> tritopic,<sup>11–15</sup> tetratopic<sup>16–21</sup> and hexatopic<sup>22–24</sup> carboxylic acids have been reported with 3,<sup>25</sup> 4,<sup>19,26</sup> 6,<sup>22</sup> 8,<sup>16,17,21</sup> 9,<sup>15,27</sup> 10,<sup>28</sup> or 12-connected<sup>7,10,18</sup>  $\text{Zr}_6$  clusters and different underlying nets. Benefiting from the aforementioned advantages, Zr-MOFs have exhibited excellent potential for various applications, including but not limited to catalysis,<sup>15,16,29</sup> chemical storage and separation,<sup>19,30</sup> sensing<sup>6,13,31</sup> and imaging.<sup>32–34</sup>

While many  $\text{Zr}_6$ -based MOFs have been synthesized since their first discovery in 2008,<sup>7</sup> those with 5-, 7- and 11-connected  $\text{Zr}_6$  clusters have rarely been reported. Likewise, although di-, tri-, tetra- and hexa-topic linkers have all been successfully used in constructing Zr-MOFs, pentacarboxylate-based structures do not exist to this date. Designing and synthesizing suitable pentacarboxylic acids to obtain corresponding Zr-MOFs have been found to be very difficult although several pentacarboxylic acids have been reported to have been used to construct Co- or Cu-MOFs more than 10 years ago.<sup>5,35,36</sup> This fact might be ascribed to the geometric frustration as reported, in which shape-mismatched linkers will prohibit the formation of predetermined frameworks.<sup>37</sup> Fortunately, the establishment and development of reticular chemistry and the Reticular Chemistry Structure Resource (RCSR) database have been proven to be useful approaches in guiding the construction of novel MOF structures *via* the top-down design and precious assembly of predesigned inorganic building units and organic linkers at the molecular level.<sup>38–45</sup> Reticular chemistry has been proven to be a useful strategy in designing many structure-<sup>9,22,46,47</sup> and property-specific<sup>48,49</sup> MOFs. Therefore, we envision that it can also

<sup>a</sup>Hoffmann Institute of Advanced Materials, Shenzhen Polytechnic University, 7098 Liuxian Blvd, Nanshan District, Shenzhen, 518055, P. R. China. E-mail: liuxiaoyuan1989@szpu.edu.cn; jingli@rutgers.edu

<sup>b</sup>College of Chemical Engineering, University of Science and Technology Liaoning, Anshan 114051, P. R. China. E-mail: gz\_xu@ustl.edu.cn

<sup>c</sup>School of Chemistry and Materials Science, Jiangsu Normal University, Xuzhou, 221116, P. R. China

<sup>d</sup>Department of Chemistry and Chemical Biology, Rutgers University, 123 Bevier Road, Piscataway, New Jersey 08854, USA

† Electronic supplementary information (ESI) available: Materials, synthesis and characterization of organic linkers and MOFs, single-crystal structures, and other additional information. Crystallographic data for the crystal structures of HIAM-4040, HIAM-4040-OH, HIAM-4040-OH-293K, HIAM-4040-OH-323K, HIAM-4040-OH-EtOH, HIAM-4040-OH-pH2 and HIAM-4040-OH-pH12. CCDC 2274419, 2290437, 2290440, 2290438, 2290436, 2290439 and 2290441. See DOI: <https://doi.org/10.1039/d3sc05410a>

‡ These authors contributed equally to this work.



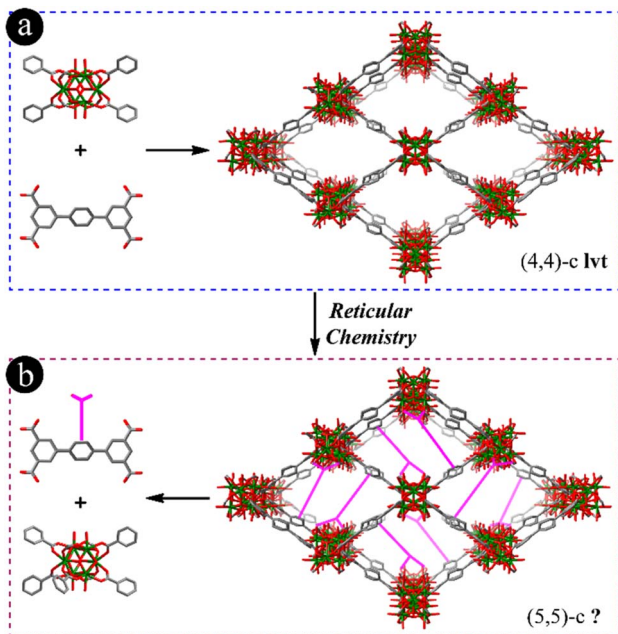


Fig. 1 (a) Molecular structure of 4-connected [1,1':4',1'']-terphenyl-3,3'',5,5''-tetracarboxylic acid (bottom left), 4-connected  $\text{Zr}_6$  cluster (top left) and single crystal structure of the corresponding MOF (lvt net, right); (b) the utilization of reticular chemistry to construct Zr-MOFs with 5-connected  $\text{Zr}_6$  clusters (bottom left) and the anticipated 5-connected linker structure (top left).

help guide the development of pentacarboxylate-based Zr-MOFs and the formation of 5-, 7-, and 11-connected  $\text{Zr}_6$  cluster-based MOFs.

As reported and shown in Fig. 1a and S1,† Zr-MOFs with 4-connected  $\text{Zr}_6$  clusters have been constructed, such as NU-1400 with an lvt underlying net using [1,1':4',1'']-terphenyl-3,3'',5,5''-tetracarboxylic acid (H<sub>4</sub>TPTC) or similar linkers.<sup>19,26</sup> In these Zr-MOFs, each linker is coordinated with four  $\text{Zr}_6$  clusters and each  $\text{Zr}_6$  cluster is connected with four linkers, leading to the formation of rhombic channels along the  $a$  axis. From the view of reticular chemistry, TPTCs are packed between two rows of 4-connected  $\text{Zr}_6$  clusters in NU-1400 viewed from the  $c$  axis (Fig. S1c†). It is thus highly possible to add another carboxylate group on the central benzene ring of TPTC to coordinate with the neighboring  $\text{Zr}_6$  cluster and block the rhombic channels as depicted in Fig. 1b, in which the 5-connected  $\text{Zr}_6$  cluster and 5-connected pentacarboxylic acid will be generated.

## Results and discussion

Bearing the aforementioned consideration in mind, two pentacarboxylic acids, 5,5'-(2-(5-carboxythiophen-2-yl)-1H-benzo[*d*]imidazole-4,7-diyl)diisophthalic acid (H<sub>5</sub>CTBII) (Fig. S2†) and 5,5'-(2-(4-carboxyphenyl)-1H-benzo[*d*]imidazole-4,7-diyl)diisophthalic acid (H<sub>5</sub>CBII) (Fig. 2a), were designed and synthesized *via* Suzuki–Miyaura coupling followed by the saponification reaction (detailed procedures in the ESI, Fig. S3–S8†) to prove our hypothesis. We then attempted to synthesize Zr-MOFs using these two linkers. For H<sub>5</sub>CTBII, no crystals were

obtained in spite of many attempts using various organic solvents and acid modulators. However, for H<sub>5</sub>CBII, single crystals with large size and uniform shape can be easily prepared. The typical synthesis procedure is as follows (Fig. 2a and b): a 5 mL vial containing H<sub>5</sub>CBII (0.018 mmol, 10.2 mg), ZrCl<sub>4</sub> (0.10 mmol, 23.3 mg), 0.8 mL formic acid and 3 mL DMF was placed in a preheated oven at 120 °C for 3 days. Colorless single crystals of HIAM-4040 were obtained with bright blue emission under 365 nm excitation (Fig. 2c and S9†) (HIAM = Hoffmann Institute of Advanced Materials; 40 = zirconium).

The single crystal X-ray diffraction (sc-XRD) analysis at 193 K indicated that HIAM-4040 crystallizes in an orthorhombic crystal system with a  $P2_12_12_1$  space group (Table S1†). As expected, each  $\text{Zr}_6\text{O}_8$  cluster in HIAM-4040 is coordinated by five fully deprotonated CBII linkers, three formate groups and four terminal  $\text{H}_2\text{O}/\text{OH}^-$  groups (Fig. 2d, S10 and S11†), which was confirmed by the <sup>1</sup>H NMR spectrum of digested HIAM-4040 (Fig. S12†). Each CBII is connected to five  $\text{Zr}_6\text{O}_8$  clusters. As a result, HIAM-4040 possesses a rarely reported (5,5)-c **zfu** topology with the overall formula of  $\text{Zr}_6\text{O}_4(\text{OH})_8(\text{H}_2\text{O})_4(\text{HCOO})_3(\text{CBII})$ . To the best of our knowledge, HIAM-4040 is the first example of Zr-MOFs constructed using a pentacarboxylate-type linker with 5-connected organic linkers and 5-connected  $\text{Zr}_6$  clusters, which is different from the reported 5-connected  $\text{Zr}_6$  cluster in NU-500, where one monodentate carboxylate ligand exists.<sup>50,51</sup> A close structure analysis demonstrates that, similar to that in NU-1400, CBII linkers are also packed between two rows of  $\text{Zr}_6$  clusters as viewed along the  $a$  axis, where additional carboxylate groups are connected to the left/below or the right/above the  $\text{Zr}_6$  cluster (Fig. S10†). As a result, the rhombic channels as observed in NU-1400 along the  $a$  axis are separated into two triangular-shaped channels and one rhombic-shaped channel along the  $b$  axis (Fig. S10,† middle). After removing the 4-(1H-imidazole-2-yl)benzoic acid group from the single crystal structure of HIAM-4040, the residual structure is almost the same as that of NU-1400 (Fig. S1 and S13†). The length of the added moiety containing carboxyl group in H<sub>5</sub>CBII is about 8.33 Å, while the distances between the central benzene ring of the organic linker and the neighboring  $\text{Zr}_6$  cluster are around 8.10 to 12.67 Å in NU-1400 under various conditions due to its flexibility. Therefore, NU-1400 can accommodate another carboxyl-contained moiety to generate the (5,5)-c underlying net. These results are consistent with our hypothesis that the 5-connected  $\text{Zr}_6$  clusters can be generated using pentacarboxylic acids based on reticular chemistry guided structural analysis of (4,4)-c lvt type Zr-MOFs, which further confirms that reticular chemistry is a powerful strategy for designing and discovering MOFs with novel structures.

To further investigate the tunability of linkers and their induced structure and property diversity, two other pentacarboxylic acids, 5,5'-(2-(4-carboxy-2-hydroxyphenyl)-1H-benzo[*d*]imidazole-4,7-diyl)diisophthalic acid (H<sub>5</sub>CHBII) (Fig. 2a) and 5,5'-(2-(4'-carboxybiphenyl-4-yl)-1H-benzo[*d*]imidazole-4,7-diyl)diisophthalic acid (H<sub>5</sub>CYBII) (Fig. S2†), were designed and synthesized *via* a similar method to H<sub>5</sub>CBII (detailed procedures in the ESI, Fig. S14–S19†). H<sub>5</sub>CHBII is the hydroxyl-functionalized H<sub>5</sub>CBII used to introduce excited-state



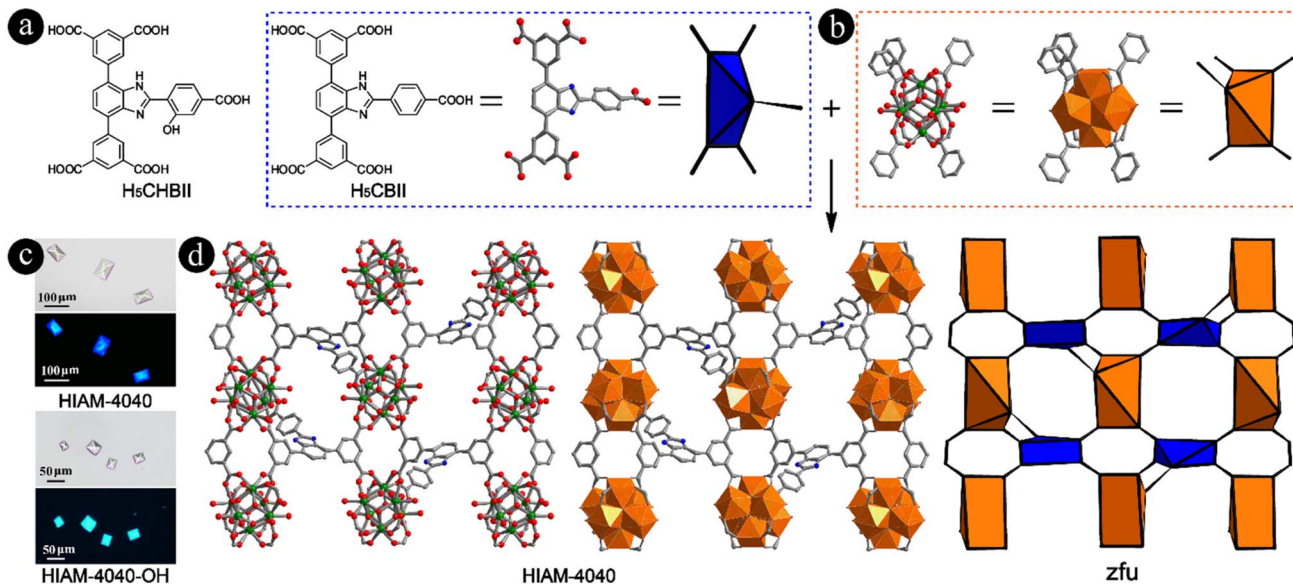


Fig. 2 (a) Schematic representation of the molecular structures of H<sub>5</sub>CHBII and H<sub>5</sub>CBII; (b) 5-connected Zr<sub>6</sub> cluster; (c) single crystal images of HIAM-4040 and HIAM-4040-OH under daylight (top) and 365 nm excitation (bottom); (d) the single-crystal structure of HIAM-4040 (color scheme: C, gray; O, red; Zr, green; N, blue).

intramolecular proton transfer (ESIPT). H<sub>5</sub>CYBII is the extension of H<sub>5</sub>CBII by incorporating an additional phenyl ring to the central benzene ring to investigate the tolerance of linker length for constructing (5,5)-c **zfu** type Zr-MOFs. As a result, light yellow single crystals (HIAM-4040-OH) were formed using H<sub>5</sub>CHBII as the organic linker, which shows bright cyan emission (Fig. 2c) with the overall formula of Zr<sub>6</sub>O<sub>4</sub>(OH)<sub>8</sub>(H<sub>2</sub>O)<sub>4</sub>-(HCOO)<sub>3</sub>(CHBII) (Fig. S20†). However, for H<sub>5</sub>CYBII, no crystals were obtained, which might be ascribed to the fact that the length of the added moiety is too large to be accommodated in the structure of NU-1400 to generate the (5,5)-c net. These results indicate that the formation of (5,5)-c **zfu** type Zr-MOFs has stringent requirements on the geometry and length of organic linkers. The sc-XRD analysis at 193 K revealed that HIAM-4040-OH also crystallizes in an orthorhombic crystal system but with a different space group, *Pnma* (Table S2†).

The phase purity of HIAM-4040 and HIAM-4040-OH was confirmed by the matched powder X-ray diffraction (PXRD) patterns between the simulated (193 K) and experimental ones (298 K) (Fig. 3a), which also reveal the isoreticular nature of HIAM-4040 and HIAM-4040-OH. A small peak shift was observed in the PXRD pattern of the activated HIAM-4040-OH sample after porosity analysis, indicative of its structural flexibility. The chemical and thermal stability of these two MOFs were also tested. As depicted in Fig. 3a and S21,† the intact PXRD patterns demonstrate that the long-range orders of HIAM-4040 and HIAM-4040-OH were well retained after treatment under various aqueous conditions, including soaking in water, in pH = 2 and 12 solutions at room temperature for 24 hours, respectively. Due to the relatively lower yield of HIAM-4040 compared with that of HIAM-4040-OH, the *in situ* temperature-dependent PXRD (TD-PXRD) and porosity measurements were conducted using HIAM-4040-OH. As

depicted in Fig. 3a and S22,† the crystallinity of HIAM-4040-OH remained unchanged even upon heating to 873 K, which is consistent with the thermogravimetric analysis (Fig. S23†). These results demonstrate that HIAM-4040 and HIAM-4040-OH have excellent chemical and thermal stability. To further confirm the framework stability, we obtained single crystal structures of HIAM-4040-OH after various treatments, namely HIAM-4040-OH-293K, HIAM-4040-OH-323K, HIAM-4040-OH-EtOH (after solvent exchange using EtOH), HIAM-4040-OH-pH2, and HIAM-4040-OH-pH12. As summarized in Tables S1 to S8,† the sc-XRD analyses not only confirm structural stability of HIAM-4040-OH upon heating and exposure to harsh chemical environments, but also indicate temperature- and solvent-dependent structural flexibility (Fig. 3a, S22 and S24†), which is similar to NU-1400.<sup>26</sup>

We attempted to analyze the permanent porosity of HIAM-4040-OH by N<sub>2</sub> and Ar sorption experiments; however negligible gas uptake was observed. We then carried out CO<sub>2</sub> sorption measurement at 195 K due to its smaller kinetic diameter compared with N<sub>2</sub> and Ar, which exhibited a type I adsorption profile (Fig. 3b). The corresponding BET surface area and total pore volume were estimated to be 308.2 m<sup>2</sup> g<sup>-1</sup> and 0.14 cm<sup>3</sup> g<sup>-1</sup>, respectively, smaller than those of NU-1400, due to the introduction of 4-(1*H*-imidazole-2-yl)benzoic acid. The pore size distribution analysis indicated two types of pores with estimated sizes of 4.5 and 6.6 Å (Fig. S25†). The experimental BET surface area and pore volume are much smaller than the calculated values of 2626.0 m<sup>2</sup> g<sup>-1</sup> and 0.56 cm<sup>3</sup> g<sup>-1</sup>, which demonstrates that only a small amount of porosity was accessible for HIAM-4040-OH.

The solid-state UV-vis absorption experiments revealed that the adsorption maxima are at 372 nm and 382 nm for HIAM-4040 and HIAM-4040-OH, respectively (Fig. 3c). The maximum



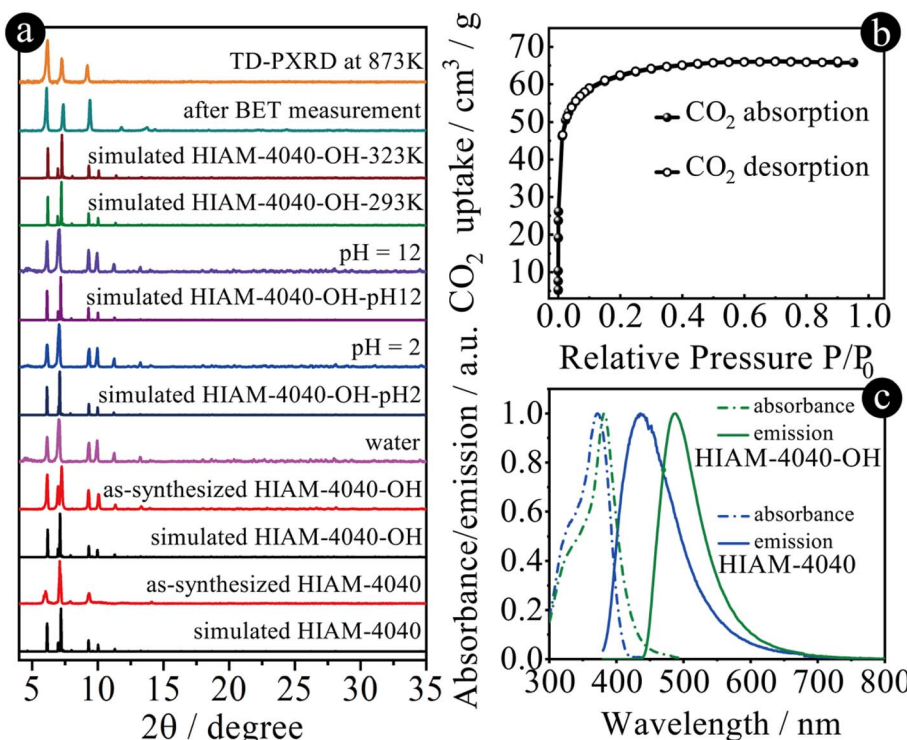


Fig. 3 (a) Simulated and experimental PXRD patterns of HIAM-4040, HIAM-4040-OH and HIAM-4040-OH after treatment under various conditions; (b) CO<sub>2</sub> adsorption–desorption isotherms at 195 K for HIAM-4040-OH; (c) solid-state emission spectra (solid lines) and UV-vis absorption spectra (dash lines) of HIAM-4040 (blue lines) and HIAM-4040-OH (green lines).

emission peaks center at 436 nm and 487 nm for HIAM-4040 and HIAM-4040-OH, respectively. It should be noticed that a Stokes shift of 105 nm was observed for HIAM-4040-OH, which is 41 nm larger than that of HIAM-4040 (64 nm). These results indicate that the introduction of a hydroxyl group triggers ESIPT and leads to red-shift emission from the keto form of CHBII under excitation (Fig. S26†),<sup>52</sup> which is the same as we have observed in the previous work.<sup>47</sup> The photoluminescence quantum yields are 24.7% and 26.3% for HIAM-4040 and HIAM-4040-OH under 365 nm excitation, respectively.

Due to strong emission and excellent chemical stability, especially in aqueous solution, HIAM-4040-OH was used to detect hypochlorous acid (HClO), one of the reactive oxygen species (ROS). HClO and other ROS and reactive nitrogen species (RNS) play an essential role in biology,<sup>53–56</sup> where the production of excess HClO is related to various diseases. Therefore, it is of great interest to monitor the concentration of HClO under aqueous conditions. The HClO concentration-dependent emission spectra were thus measured by gradual addition of HClO into the aqueous suspension of HIAM-4040-OH. As shown in Fig. 4a, the emission at 490 nm of HIAM-4040-OH gradually decreased with an increasing concentration of HClO. This result is consistent with the decreased emission lifetime of HIAM-4040-OH after addition of HClO (Fig. 4b), which decreased from 2.00 ns to 1.58 ns and 1.24 ns when 300 and 600 μM HClO was added. The emission intensity of HIAM-4040-OH showed a linear correlation coefficient of 0.998 toward the concentration of HClO in the range of 0 to

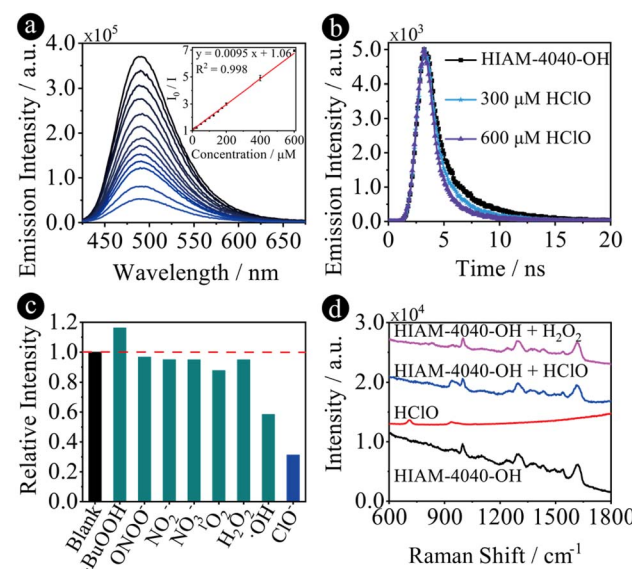


Fig. 4 (a) The concentration-dependent emission quenching of HIAM-4040-OH with HClO concentrations of 5, 15, 25, 50, 75, 100, 125, 150, 175, 200, 400 and 600 μM, and the corresponding Stern–Volmer plot; (b) the fluorescence lifetime decay profiles of HIAM-4040-OH before and after addition of HClO; (c) the selectivity test of HIAM-4040-OH with different kinds of ROS and RNS; (d) the Raman spectra of HIAM-4040-OH before and after treatment using HClO and H<sub>2</sub>O<sub>2</sub>.

0.6 mM with a calculated detection limitation of 1.57  $\mu$ M, which is comparable with those of the reported MOF-based materials for HClO detection (Table S9†). A similar emission quenching behavior was also observed for HIAM-4040 after adding HClO (Fig. S27†). HIAM-4040-OH also exhibited high selectivity towards HClO compared with other RNS and ROS, including t-BuOOH,  $\text{ONOO}^-$ ,  $\text{NO}_2^-$ ,  $\text{NO}_3^-$ ,  ${}^1\text{O}_2$ ,  $\text{H}_2\text{O}_2$  and  $\cdot\text{OH}$  (Fig. 4c). Moreover, the well matched PXRD patterns of the simulated HIAM-4040-OH and as-synthesized HIAM-4040-OH, after grinding and detection of HClO indicate the excellent stability of HIAM-4040-OH (Fig. S28†). These results demonstrate that HIAM-4040-OH can be used for highly sensitive and selective detection of HClO in aqueous solutions.

To understand the turn-off sensing mechanism of HIAM-4040-OH toward HClO, several control experiments were conducted. (i) The similar emission quenching behavior of HIAM-4040 and HIAM-4040-OH upon the addition of HClO indicates that the OH group on the linker skeleton of HIAM-4040-OH is not the reaction site for the turn-off mechanism (Fig. S27†). (ii) Almost no change was observed for the emission of HIAM-4040-OH when HCl was added, indicating that the emission quenching is not from the acidic nature of HClO (Fig. S29†). (iii) A slight emission decrease was recorded when HClO was added into a benzothiadiazole-based luminescent MOF solution, HIAM-4011,<sup>57</sup> which demonstrates that the N atom on the benzothiadiazole is silent toward HClO (Fig. S30†). (iv) The UV-vis absorption range of HClO is less than 350 nm, ruling out the energy transfer induced emission quenching between HIAM-4040-OH and HClO (Fig. S31†). According to the aforementioned experiments, we conclude that the reason for the turn-off emission is the reaction between HClO and the NH group on the imidazole ring. As a strong oxidizing agent, the NH group will be oxidized to N after adding HClO to HIAM-4040-OH solution, where the electrons will rearrange to generate a carbon radical, which will quench the emission of HIAM-4040-OH. To confirm our hypothesis, the Raman spectra of HIAM-4040-OH before and after adding HClO were measured. As shown in Fig. 4d, the typical Raman peaks at 998, 1295 and 1617  $\text{cm}^{-1}$  were attributed to the trigonal bending, C–N and C=C stretching vibrations of linkers in HIAM-4040-OH. After addition of HClO, a new Raman peak originating from C–N–C appeared at 940  $\text{cm}^{-1}$  and was attributed to the oxidation of N–H on the imidazole ring, while no peak at 940  $\text{cm}^{-1}$  was observed when  $\text{H}_2\text{O}_2$  was added, which further confirms that only HClO has this specific interaction with HIAM-4040-OH.

## Conclusion

In conclusion, we report the successful application of reticular chemistry to construct pentacarboxylate-based Zr-MOFs, HIAM-4040 and HIAM-4040-OH, inspired by (4,4)-c Ivt type Zr-MOFs. To the best of our knowledge, this is the first Zr-pentacarboxylate framework and the first study disclosing a 5-connected organic linker and 5-connected  $\text{Zr}_6$  node. By introducing a hydroxyl group into the linker skeleton of HIAM-4040, an isoreticular structure, HIAM-4040-OH, is generated with a larger Stokes shift *via* ESIPT. Due to its excellent chemical and

thermal stability, HIAM-4040-OH was utilized for HClO detection in an aqueous solution with high sensitivity and selectivity. This work points to a new avenue for rationally designing and constructing Zr-MOFs with unique structures guided by reticular chemistry.

## Data availability

All the data can be found in the main article and ESI.†

## Author contributions

X. Y. L. conceived the idea and designed the experiment; T. Peng and C.-Q. Han worked on the synthesis and the characterization of all materials. H.-L. Xia and K. Zhou obtained and analyzed the single crystal structures. J. Zhang, J. Si, L. Wang and L.-L. Qu performed the data analysis of HClO detection. J. Miao, F.-A. Guo and H. Wang obtained the adsorption–desorption isotherms. X.-Y. L., J. Li and G. Xu wrote the paper with help from all authors. T. Peng and C.-Q. Han contributed equally to this work.

## Conflicts of interest

The authors declare no competing financial interests.

## Acknowledgements

X.-Y. Liu acknowledges the financial support from the National Natural Science Foundation of China (grant no. 22201185), Guangdong Basic and Applied Basic Research Foundation (grant no. 2023A1515011494) and Shenzhen Science and Technology Program (20231123083040001). L. Wang gratefully acknowledges the financial support from the Post-Doctoral Foundation Project of Shenzhen Polytechnic (6022331004K).

## References

- 1 Y. Bai, Y. Dou, L. H. Xie, W. Rutledge, J. R. Li and H. C. Zhou, Zr-based metal-organic frameworks: design, synthesis, structure, and applications, *Chem. Soc. Rev.*, 2016, **45**(8), 2327–2367.
- 2 S. Yuan, J.-S. Qin, C. T. Lollar and H.-C. Zhou, Stable Metal-Organic Frameworks with Group 4 Metals: Current Status and Trends, *ACS Cent. Sci.*, 2018, **4**(4), 440–450.
- 3 Z. Chen, S. L. Hanna, L. R. Redfern, D. Alezi, T. Islamoglu and O. K. Farha, Reticular chemistry in the rational synthesis of functional zirconium cluster-based MOFs, *Coord. Chem. Rev.*, 2019, **386**, 32–49.
- 4 C. W. Kung, S. Goswami, I. Hod, T. C. Wang, J. Duan, O. K. Farha and J. T. Hupp, Charge Transport in Zirconium-Based Metal-Organic Frameworks, *Acc. Chem. Res.*, 2020, **53**(6), 1187–1195.
- 5 H. Ghasempour, K.-Y. Wang, J. A. Powell, F. ZareKarizi, X.-L. Lv, A. Morsali and H.-C. Zhou, Metal-organic frameworks based on multicarboxylate linkers, *Coord. Chem. Rev.*, 2021, **426**, 213542.



- 6 C. Jia, T. He and G.-M. Wang, Zirconium-based metal-organic frameworks for fluorescent sensing, *Coord. Chem. Rev.*, 2023, **476**, 214930.
- 7 J. H. Cavka, S. Jakobsen, U. Olsbye, N. Guillou, C. Lamberti, S. Bordiga and K. P. Lillerud, A New Zirconium Inorganic Building Brick Forming Metal Organic Frameworks with Exceptional Stability, *J. Am. Chem. Soc.*, 2008, **130**(42), 13850–13851.
- 8 S. Yuan, W. Lu, Y. P. Chen, Q. Zhang, T. F. Liu, D. Feng, X. Wang, J. Qin and H. C. Zhou, Sequential linker installation: precise placement of functional groups in multivariate metal-organic frameworks, *J. Am. Chem. Soc.*, 2015, **137**(9), 3177–3180.
- 9 V. Guillerm, T. Grancha, I. Imaz, J. Juanhuix and D. Maspoch, Zigzag Ligands for Transversal Design in Reticular Chemistry: Unveiling New Structural Opportunities for Metal–Organic Frameworks, *J. Am. Chem. Soc.*, 2018, **140**(32), 10153–10157.
- 10 N. Alsadun, G. Mouchaham, V. Guillerm, J. Czaban-Józwiak, A. Shkurenko, H. Jiang, P. M. Bhatt, P. Parvatkar and M. Eddaoudi, Introducing a Cantellation Strategy for the Design of Mesoporous Zeolite-like Metal–Organic Frameworks: Zr-sod-ZMOFs as a Case Study, *J. Am. Chem. Soc.*, 2020, **142**(49), 20547–20553.
- 11 H. Furukawa, F. Gándara, Y.-B. Zhang, J. Jiang, W. L. Queen, M. R. Hudson and O. M. Yaghi, Water Adsorption in Porous Metal–Organic Frameworks and Related Materials, *J. Am. Chem. Soc.*, 2014, **136**(11), 4369–4381.
- 12 D. Feng, K. Wang, J. Su, T.-F. Liu, J. Park, Z. Wei, M. Bosch, A. Yakovenko, X. Zou and H.-C. Zhou, A Highly Stable Zeotype Mesoporous Zirconium Metal–Organic Framework with Ultralarge Pores, *Angew. Chem., Int. Ed.*, 2015, **54**(1), 149–154.
- 13 B. Wang, X. L. Lv, D. Feng, L. H. Xie, J. Zhang, M. Li, Y. Xie, J. R. Li and H. C. Zhou, Highly Stable Zr(IV)-Based Metal–Organic Frameworks for the Detection and Removal of Antibiotics and Organic Explosives in Water, *J. Am. Chem. Soc.*, 2016, **138**(19), 6204–6216.
- 14 S. Lee, H.-B. Bürgi, S. A. Alshimimri and O. M. Yaghi, Impact of Disordered Guest–Framework Interactions on the Crystallography of Metal–Organic Frameworks, *J. Am. Chem. Soc.*, 2018, **140**(28), 8958–8964.
- 15 Y. Zhao, S. Qi, Z. Niu, Y. Peng, C. Shan, G. Verma, L. Wojtas, Z. Zhang, B. Zhang, Y. Feng, Y.-S. Chen and S. Ma, Robust Corrole-Based Metal–Organic Frameworks with Rare 9-Connected Zr/Hf-Oxo Clusters, *J. Am. Chem. Soc.*, 2019, **141**(36), 14443–14450.
- 16 D. Feng, Z. Y. Gu, J. R. Li, H. L. Jiang, Z. Wei and H. C. Zhou, Zirconium-metallocporphyrin PCN-222: mesoporous metal-organic frameworks with ultrahigh stability as biomimetic catalysts, *Angew. Chem., Int. Ed.*, 2012, **51**(41), 10307–10310.
- 17 J. E. Mondloch, W. Bury, D. Fairen-Jimenez, S. Kwon, E. J. DeMarco, M. H. Weston, A. A. Sarjeant, S. T. Nguyen, P. C. Stair, R. Q. Snurr, O. K. Farha and J. T. Hupp, Vapor-Phase Metalation by Atomic Layer Deposition in a Metal–Organic Framework, *J. Am. Chem. Soc.*, 2013, **135**(28), 10294–10297.
- 18 T. C. Wang, W. Bury, D. A. Gómez-Gualdrón, N. A. Vermeulen, J. E. Mondloch, P. Deria, K. Zhang, P. Z. Moghadam, A. A. Sarjeant, R. Q. Snurr, J. F. Stoddart, J. T. Hupp and O. K. Farha, Ultrahigh Surface Area Zirconium MOFs and Insights into the Applicability of the BET Theory, *J. Am. Chem. Soc.*, 2015, **137**(10), 3585–3591.
- 19 H. Wang, X. Dong, J. Lin, S. J. Teat, S. Jensen, J. Cure, E. V. Alexandrov, Q. Xia, K. Tan, Q. Wang, D. H. Olson, D. M. Proserpio, Y. J. Chabal, T. Thonhauser, J. Sun, Y. Han and J. Li, Topologically guided tuning of Zr-MOF pore structures for highly selective separation of C6 alkane isomers, *Nat. Commun.*, 2018, **9**(1), 1745.
- 20 S. Wang, J. S. Lee, M. Wahiduzzaman, J. Park, M. Muschi, C. Martineau-Corcos, A. Tissot, K. H. Cho, J. Marrot, W. Shepard, G. Maurin, J.-S. Chang and C. Serre, A robust large-pore zirconium carboxylate metal–organic framework for energy-efficient water-sorption-driven refrigeration, *Nat. Energy*, 2018, **3**(11), 985–993.
- 21 X. L. Lv, S. Yuan, L. H. Xie, H. F. Darke, Y. Chen, T. He, C. Dong, B. Wang, Y. Z. Zhang, J. R. Li and H. C. Zhou, Ligand Rigidification for Enhancing the Stability of Metal–Organic Frameworks, *J. Am. Chem. Soc.*, 2019, **141**(26), 10283–10293.
- 22 D. Alezi, I. Spanopoulos, C. Tsangarakis, A. Shkurenko, K. Adil, Y. Belmabkhout, M. O’Keeffe, M. Eddaoudi and P. N. Trikalitis, Reticular Chemistry at Its Best: Directed Assembly of Hexagonal Building Units into the Awaited Metal–Organic Framework with the Intricate Polybenzene Topology, pbz-MOF, *J. Am. Chem. Soc.*, 2016, **138**(39), 12767–12770.
- 23 J.-S. Qin, S. Yuan, L. Zhang, B. Li, D.-Y. Du, N. Huang, W. Guan, H. F. Drake, J. Pang, Y.-Q. Lan, A. Alsalme and H.-C. Zhou, Creating Well-Defined Hexabenzocoronene in Zirconium Metal–Organic Framework by Postsynthetic Annulation, *J. Am. Chem. Soc.*, 2019, **141**(5), 2054–2060.
- 24 Z. Chen, P. Li, X. Wang, K.-i. Otake, X. Zhang, L. Robison, A. Atilgan, T. Islamoglu, M. G. Hall, G. W. Peterson, J. F. Stoddart and O. K. Farha, Ligand-Directed Reticular Synthesis of Catalytically Active Missing Zirconium-Based Metal–Organic Frameworks, *J. Am. Chem. Soc.*, 2019, **141**(31), 12229–12235.
- 25 T.-H. Chen, I. Popov and O. Š. Miljanić, A Zirconium Macrocyclic Metal–Organic Framework with Predesigned Shape-Persistent Apertures, *Chem.-Eur. J.*, 2017, **23**(2), 286–290.
- 26 Y. Zhang, X. Zhang, J. Lyu, K. I. Otake, X. Wang, L. R. Redfern, C. D. Malliakas, Z. Li, T. Islamoglu, B. Wang and O. K. Farha, A Flexible Metal–Organic Framework with 4-Connected Zr<sub>6</sub> Nodes, *J. Am. Chem. Soc.*, 2018, **140**(36), 11179–11183.
- 27 T. He, Y.-Z. Zhang, X.-J. Kong, J. Yu, X.-L. Lv, Y. Wu, Z.-J. Guo and J.-R. Li, Zr(IV)-Based Metal–Organic Framework with T-Shaped Ligand: Unique Structure, High Stability, Selective Detection, and Rapid Adsorption of Cr<sub>2</sub>O<sub>7</sub><sup>2-</sup> in Water, *ACS Appl. Mater. Interfaces*, 2018, **10**(19), 16650–16659.



- 28 V. Bon, I. Senkovska, I. A. Baburin and S. Kaskel, Zr- and Hf-Based Metal–Organic Frameworks: Tracking Down the Polymorphism, *Cryst. Growth Des.*, 2013, **13**(3), 1231–1237.
- 29 W. Gong, X. Chen, H. Jiang, D. Chu, Y. Cui and Y. Liu, Highly Stable Zr(IV)-Based Metal–Organic Frameworks with Chiral Phosphoric Acids for Catalytic Asymmetric Tandem Reactions, *J. Am. Chem. Soc.*, 2019, **141**(18), 7498–7508.
- 30 C. X. Chen, Z. W. Wei, J. J. Jiang, S. P. Zheng, H. P. Wang, Q. F. Qiu, C. C. Cao, D. Fenske and C. Y. Su, Dynamic Spacer Installation for Multirole Metal–Organic Frameworks: A New Direction toward Multifunctional MOFs Achieving Ultrahigh Methane Storage Working Capacity, *J. Am. Chem. Soc.*, 2017, **139**(17), 6034–6037.
- 31 J. Li, S. Yuan, J.-S. Qin, J. Pang, P. Zhang, Y. Zhang, Y. Huang, H. F. Drake, W. R. Liu and H.-C. Zhou, Stepwise Assembly of Turn-on Fluorescence Sensors in Multicomponent Metal–Organic Frameworks for in Vitro Cyanide Detection, *Angew. Chem., Int. Ed.*, 2020, **59**(24), 9319–9323.
- 32 J. Park, Q. Jiang, D. Feng, L. Mao and H. C. Zhou, Size-Controlled Synthesis of Porphyrinic Metal–Organic Framework and Functionalization for Targeted Photodynamic Therapy, *J. Am. Chem. Soc.*, 2016, **138**(10), 3518–3525.
- 33 J. Park, M. Xu, F. Li and H. C. Zhou, 3D Long-Range Triplet Migration in a Water-Stable Metal–Organic Framework for Upconversion-Based Ultralow-Power in Vivo Imaging, *J. Am. Chem. Soc.*, 2018, **140**(16), 5493–5499.
- 34 B. Li, X. Lu, Y. Tian and D. Li, Embedding Multiphoton Active Units within Metal–Organic Frameworks for Turning on High-Order Multiphoton Excited Fluorescence for Bioimaging, *Angew. Chem., Int. Ed.*, 2022, **61**(31), e202206755.
- 35 J. K. Schnobrich, O. Lebel, K. A. Cychosz, A. Dailly, A. G. Wong-Foy and A. J. Matzger, Linker-Directed Vertex Desymmetrization for the Production of Coordination Polymers with High Porosity, *J. Am. Chem. Soc.*, 2010, **132**(39), 13941–13948.
- 36 L. Bai, H.-B. Wang, D.-S. Li, Y.-P. Wu, J. Zhao and L.-F. Ma, A new penta-carboxylate and N-donor ligand co-regulate 3D CoII-MOF with tcj/hc topology: Synthesis, structure and magnetic property, *Inorg. Chem. Commun.*, 2014, **44**, 188–190.
- 37 F. Haase, G. A. Craig, M. Bonneau, K. Sugimoto and S. Furukawa, Pseudo-5-Fold-Symmetrical Ligand Drives Geometric Frustration in Porous Metal–Organic and Hydrogen-Bonded Frameworks, *J. Am. Chem. Soc.*, 2020, **142**(32), 13839–13845.
- 38 N. W. Ockwig, O. Delgado-Friedrichs, M. O’Keeffe and O. M. Yaghi, Reticular Chemistry: Occurrence and Taxonomy of Nets and Grammar for the Design of Frameworks, *Acc. Chem. Res.*, 2005, **38**(3), 176–182.
- 39 M. O’Keeffe, M. A. Peskov, S. J. Ramsden and O. M. Yaghi, The Reticular Chemistry Structure Resource (RCSR) Database of, and Symbols for, Crystal Nets, *Acc. Chem. Res.*, 2008, **41**(12), 1782–1789.
- 40 D. J. Tranchemontagne, Z. Ni, M. O’Keeffe and O. M. Yaghi, Reticular Chemistry of Metal–Organic Polyhedra, *Angew. Chem., Int. Ed.*, 2008, **47**(28), 5136–5147.
- 41 O. M. Yaghi, M. J. Kalmutzki and C. S. Diercks, *Introduction to Reticular Chemistry*, Wiley, 2019, pp. 1–509.
- 42 Y. Liu, M. O’Keeffe, M. M. J. Treacy and O. M. Yaghi, The geometry of periodic knots, polycatenanes and weaving from a chemical perspective: a library for reticular chemistry, *Chem. Soc. Rev.*, 2018, **47**(12), 4642–4664.
- 43 V. Guillerm and D. Maspoch, Geometry Mismatch and Reticular Chemistry: Strategies To Assemble Metal–Organic Frameworks with Non-default Topologies, *J. Am. Chem. Soc.*, 2019, **141**(42), 16517–16538.
- 44 H. Lyu, Z. Ji, S. Wuttke and O. M. Yaghi, Digital Reticular Chemistry, *Chem.*, 2020, **6**(9), 2219–2241.
- 45 M. J. Kalmutzki, N. Hanikel and O. M. Yaghi, Secondary building units as the turning point in the development of the reticular chemistry of MOFs, *Sci. Adv.*, 2018, **4**(10), eaat9180.
- 46 N. R. Catarineu, A. Schoedel, P. Urban, M. B. Morla, C. A. Trickett and O. M. Yaghi, Two Principles of Reticular Chemistry Uncovered in a Metal–Organic Framework of Heterotritopic Linkers and Infinite Secondary Building Units, *J. Am. Chem. Soc.*, 2016, **138**(34), 10826–10829.
- 47 J. Si, H.-L. Xia, K. Zhou, J. Li, K. Xing, J. Miao, J. Zhang, H. Wang, L.-L. Qu, X.-Y. Liu and J. Li, Reticular Chemistry with Art: A Case Study of Olympic Rings-Inspired Metal–Organic Frameworks, *J. Am. Chem. Soc.*, 2022, **144**(48), 22170–22177.
- 48 C. S. Diercks, Y. Liu, K. E. Cordova and O. M. Yaghi, The role of reticular chemistry in the design of CO<sub>2</sub> reduction catalysts, *Nat. Mater.*, 2018, **17**(4), 301–307.
- 49 S. M. Towsif Abtab, D. Alezi, P. M. Bhatt, A. Shkurenko, Y. Belmabkhout, H. Aggarwal, Ł. J. Weseliński, N. Alsadun, U. Samin, M. N. Hedhili and M. Eddaoudi, Reticular Chemistry in Action: A Hydrolytically Stable MOF Capturing Twice Its Weight in Adsorbed Water, *Chem.*, 2018, **4**(1), 94–105.
- 50 Y. Chen, X. Zhang, M. R. Mian, F. A. Son, K. Zhang, R. Cao, Z. Chen, S. J. Lee, K. B. Idrees, T. A. Goetjen, J. Lyu, P. Li, Q. Xia, Z. Li, J. T. Hupp, T. Islamoglu, A. Napolitano, G. W. Peterson and O. K. Farha, Structural Diversity of Zirconium Metal–Organic Frameworks and Effect on Adsorption of Toxic Chemicals, *J. Am. Chem. Soc.*, 2020, **142**(51), 21428–21438.
- 51 D. Nam, J. Kim and W. Choe, Evolution of Zr nodes in metal–organic frameworks, *Trends Chem.*, 2023, **5**(5), 339–352.
- 52 V. S. Padalkar and S. Seki, Excited-state intramolecular proton-transfer (ESIPT)-inspired solid state emitters, *Chem. Soc. Rev.*, 2016, **45**(1), 169–202.
- 53 C. C. Winterbourn, M. B. Hampton, J. H. Livesey and A. J. Kettle, Modeling the Reactions of Superoxide and Myeloperoxidase in the Neutrophil Phagosome: Implications for Microbial Killing, *J. Biochem.*, 2006, **281**(52), 39860–39869.
- 54 S. G. Rhee, H<sub>2</sub>O<sub>2</sub>, a Necessary Evil for Cell Signaling, *Science*, 2006, **312**(5782), 1882–1883.



- 55 D. I. Pattison and M. J. Davies, Evidence for Rapid Inter- and Intramolecular Chlorine Transfer Reactions of Histamine and Carnosine Chloramines: Implications for the Prevention of Hypochlorous-Acid-Mediated Damage, *Biochemistry*, 2006, **45**(26), 8152–8162.
- 56 F. C. Fang, Antimicrobial reactive oxygen and nitrogen species: concepts and controversies, *Nat. Rev. Microbiol.*, 2004, **2**(10), 820–832.
- 57 H.-L. Xia, K. Zhou, L. Yu, H. Wang, X.-Y. Liu, D. M. Proserpio and J. Li, Customized Synthesis: Solvent- and Acid-Assisted Topology Evolution in Zirconium-Tetracarboxylate Frameworks, *Inorg. Chem.*, 2022, **61**(20), 7980–7988.

